Dynamic external dose assessment by LES modeling of radioactive pollutant dispersion over an open field

Lieven Vervecken[1,2], Johan Camps[1], Johan Meyers[2]

Abstract

Performing accurate doses assessments are an essential part of the nuclear emergency preparedness and response phases. To improve the dose estimation at the near-range and assess the dynamic behavior, a model is developed in this work using CFD. The evolution of the concentration is formulated as a transient convection-diffusion problem in which the instantaneous profiles for velocity and eddy viscosity are produced by a large eddy simulation of the atmospheric boundary layer. The beta and gamma dose rates are computed from the local concentration and using the point-kernel method with buildup factors, respectively.
The model is applied to the dispersion of the unstable isotopes Argon-41 and Xenon-133, released over an open field under neutral atmospheric stratification. It is observed that even under constant pollutant emission rate, strongly fluctuating beta and dose rates in time are registered, regardless the isotope. Furthermore, the results point out that the gamma dose assessment at the near-range is not representative for the external beta dose rate.

Introduction

An essential part of the nuclear emergency preparedness and response phases is the estimation of the external dose to the general public after the release of radioactive gases. This is in particular important in order to be able to take effective countermeasures. Although Gaussian models are frequently used to assess atmospheric pollutant dispersion after accidental releases (e.g., Venkatesan et al., 2002; Benamrane et al., 2013), they are known to have a limited accuracy close to the source or in situations with complex air flow (Punitha et al., 2008; Nakayama and Nagai, 2009). One alternative in these situations is the use of Computational Fluid Dynamics (CFD) using Large-Eddy Simulation (LES) turbulence modeling (e.g., de Sampaio et al., 2008; Nakayama and Nagai, 2009). The strength of this method is that the variability of the atmospheric boundary layer can be accounted for in the dispersion simulation without the need for highly temporal meteorological wind field data which would be required for, for example, Gaussian puff models and particle models (Rentai, 2011).

Therefore, by coupling a LES model with a beta and gamma dose rate model, not only an improved accuracy is obtained, but also the dynamic behavior of the external dose rate from beta and gamma radiation can be assessed. Such an assessment can be particularly useful when studying the optimization of measurement strategies, and when estimating measurement uncertainties related to atmospheric effects. The particular focus of the current work is on studying the differences between the dynamics of the beta and gamma dose rates from cloud

[1] SCK•CEN, Belgian Nuclear Research Centre, Boeretang 200, 2400 Mol (Belgium)
[2] Department of Mechanical Engineering, KU Leuven, Celestijnenlaan 300, 3000 Leuven (Belgium)

shine. To this end, we simulate the dispersion of ^{41}Ar and ^{133}Xe over an open field and monitor the external dose rate at ground level.

Method

We use an Eulerian approach to simulate the pollutant dispersion from a stack release over an open field under neutral atmospheric stratification. The evolution of the concentration is formulated as a transient three-dimensional convection-diffusion problem with the sub-grid scale (SGS) pollutant flux modeled based on an eddy-diffusivity approach:

$$\frac{\partial c}{\partial t} + \nabla \cdot (\boldsymbol{u}c) = \nabla \cdot \frac{\nu_{sgs}}{Sc_{sgs}} \nabla c - \lambda c + S \tag{1}$$

where c is the pollutant concentration, $\mathbf{u}$ is the wind field, $\mathrm{Sc_{sgs}}$ is the SGS Schmidt number which is set equal to 0.4 (Chamecki et al., 2009), ν_{sgs} is the SGS eddy viscosity, λ is the radioactive decay constant, and S is the pollutant source. Note that the pollutant source can either be a localized point source such as a stack release, or a distributed source such as the radioactive decay of a dispersed parent isotope. In order to impose a realistic representation of the wind field, the instantaneous profiles for velocity and eddy viscosity are produced by a large eddy simulation of the atmospheric boundary layer. In this work, the Lagrangian scale-dependent dynamic model as introduced by Bou-Zeid et al. (2005), is used to evaluate the SGS viscosity.

Because of the limited range of β particles in air (Berger et al., 2000), the beta dose at a location $\mathbf{x}_0 = (\mathrm{x}', \mathrm{y}', \mathrm{z}')$ can be estimated by treating the plume as an infinite cloud with a concentration equal to the local concentration. This allows the beta dose rate in air to be computed as (Slade, 1968):

$$\dot{\mathrm{d}}_{\beta,\mathbf{x}_0} = \mathrm{K}_\beta \overline{\mathrm{E}}_\beta \lambda \mathrm{c}(\mathrm{x}_0) \tag{2}$$

with K_β a conversion factor accounting for the properties of air, $\overline{\mathrm{E}}_\beta$ the average beta energy per disintegration, and $\mathrm{c}(\mathbf{x}_0)$ the concentration at location $\mathbf{x}_0$. The surface body dose rate can be approximated by one-half of $\dot{\mathrm{d}}_{\beta,\mathrm{x}_0}$ (Slade, 1968).

The gamma dose rate at location $\mathbf{x}_0$ is computed from the gamma fluence rate. Using the point-kernel method with buildup factors, the latter can be evaluated as

$$\phi_{\mathbf{x}_0} = \iiint_{\mathrm{V}} \frac{\mathrm{B}(\mu,\mathrm{r})}{4\pi \mathrm{r}^2} \mathrm{e}^{-\mu \mathrm{r}} \lambda \mathrm{c}\, \mathrm{dx}'\mathrm{dy}'\mathrm{dz}' \tag{3}$$

where $\mathrm{r}^2 = (\mathrm{x}_0 - \mathrm{x}')^2 + (\mathrm{y}_0 - \mathrm{y}')^2 + (\mathrm{z}_0 - \mathrm{z}')^2$, V is the domain volume, μ is the linear attenuation coeffcient in air and B is the dose build-up factor. To evaluate B, we employ the parameterization in Taylor form (ANSI, 1991). Conversion of the local fluence rate into the local dose rate to a material can subsequently be achieved as

$$\dot{\mathrm{d}}_{\gamma,\mathbf{x}_0} = \frac{\mathrm{E}_\gamma \mu_{\mathrm{en}}}{\rho} \phi_{\mathbf{x}_0} \tag{4}$$

with E_γ the gamma energy released per disintegration, μ_{en} the energy absorption coefficient and ρ the density of the receptor. Hence, the resulting gamma dose rate is directly proportional to the gamma fluence rate.

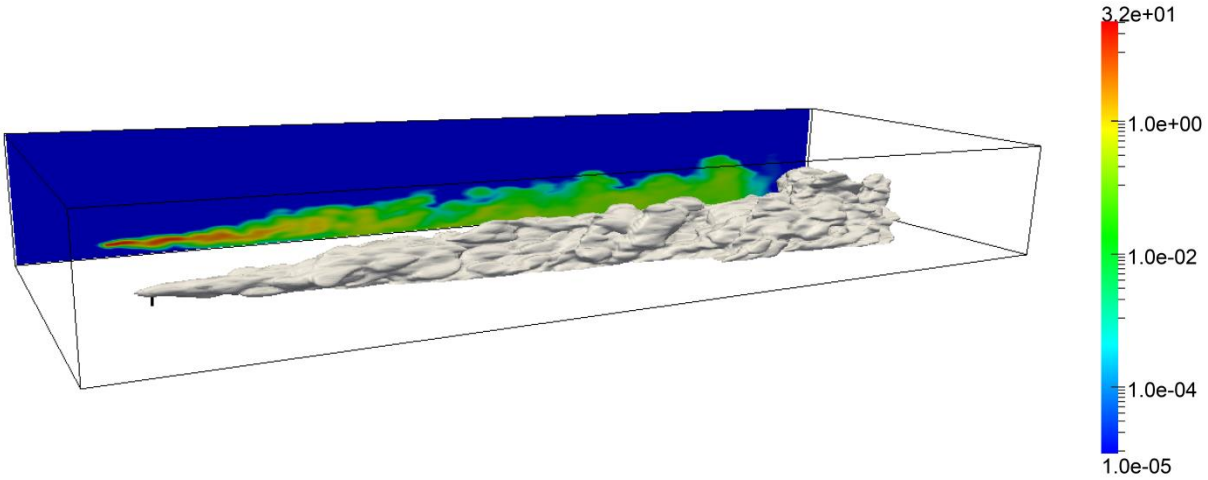

Figure 1: Instantaneous concentration c^*, released from 75 m altitude. In gray, isosurface for $c^* = 10^{-5}$; Back plane, concentration in the stream-wise, vertical cross section through the point of release.

Computational set-up

The geometry of the cases simulated is very simple, i.e. an open field without any obstructions from buildings or vegetation. The simulation domain chosen is of size 6 km × 1.5 km × 750 m. We position the pollutant source 500 m downstream from the inlet boundary, and in the middle of the domain in crosswind direction. The pollutant is released at a constant rate from 75 m altitude and the dose rates are monitored at 1.5 m.

The model is applied to the dispersion of the unstable isotopes ^{41}Ar and ^{133}Xe, both frequently emitted in various nuclear facilities. These gases are chemically highly nonreactive and they do not deposit. A high energy gamma of $\mathrm{E}_\gamma = 1\,293.64$ keV is emitted when ^{41}Ar decays by beta minus decay with a decay constant of 105.36×10^{-6} s^{-1} (Bé et al., 2011). Conversely, a low energy gamma of $\mathrm{E}_\gamma = 81.0$ keV is emitted during the beta minus decay of ^{133}Xe. The decay constant of this process is 1.53×10^{6} s^{-1} (Bé et al., 2008).

The dose assessment problem is simulated using the OpenFOAM finite-volume open-source simulation platform. The transport equations are discretized on a uniformly spaced, hexahedral mesh consisting of 11.7 million cells using second-order schemes in space and time. Further, instead of reporting the beta and gamma dose rates, we bound ourselves to a discussion of the local concentration and the gamma fluence rate, respectively, to eliminate the effect of the receptor characteristics on the result. Finally, we normalize time, distance, concentration and fluence rate in this study as

$$t^* = t\frac{U}{L} \quad x^* = \frac{x}{L} \quad c^* = c\frac{UL^2}{R} \quad \phi^* = \phi\frac{L^2}{R} \tag{5}$$

where R is the release rate, L is the release height, U is the mean wind speed at an altitude L according to the logarithmic profile.

Results and discussion

A typical result of the dispersion model is shown in Fig. 1 as an instantaneous, three-dimensional isosurface of the concentration $c^* = 10^{-5}$. Clearly, the turbulent nature of the boundary layer results in a non-uniform plume with a spread increasing with the distance from

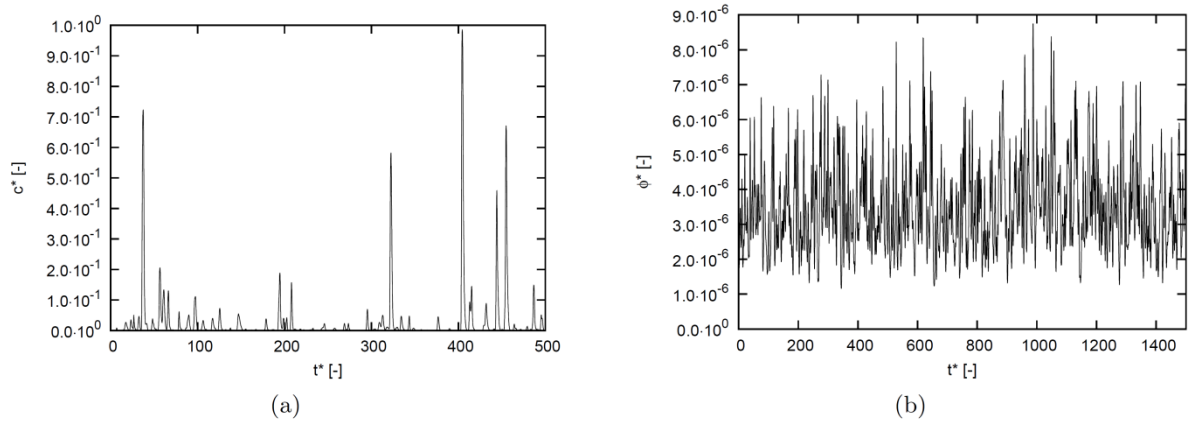

Figure 2: Observed concentration c^* (a), and gamma uence rate ϕ^* (b), at $x^* = 10$ due to the emission of ^{133}Xe from 75 m altitude.

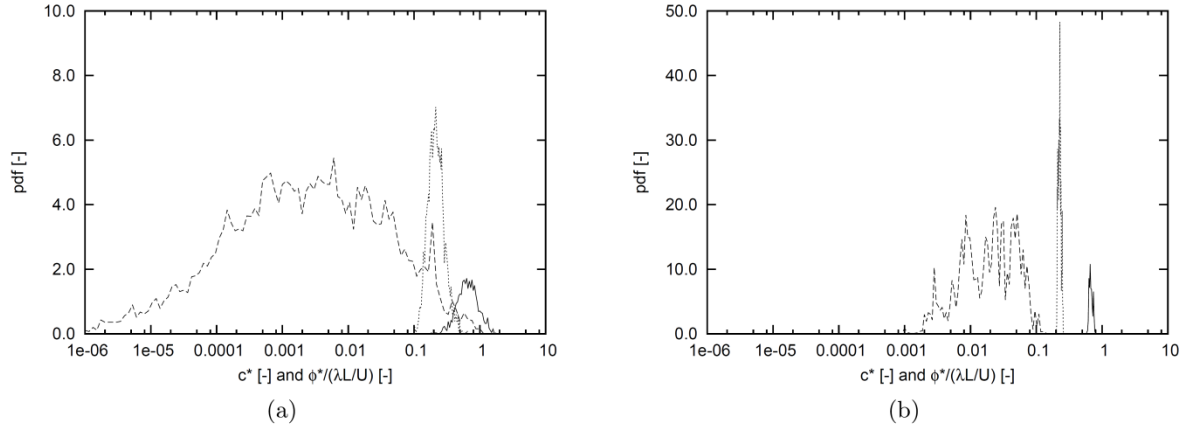

Figure 3: Probability density function of the concentration c^* $(--)$ and the gamma fluence rates ϕ^* of ^{41}Ar $(\cdots)$, and ^{133}Xe $(-)$; (a) instantaneous, (b) time-averaged with $\Delta t^* = 125$.

the point of release. When looking at the concentration in the vertical cross section through the point of release, plotted on the back plane of Fig. 1 (the plane is offset for the sake of visualization), we find that the concentration is the largest in the direct proximity of the pollutant source and strongly decreases with downwind distance. Halfway the domain, the peak concentration has dropped two orders of magnitude with respect to the maximum concentration, found close to the pollutant source.

The local concentration and gamma fluence rates observed at a distance $x^* = 10$ from the emission of ^{133}Xe are shown in Fig. 2 as a function of the non-dimensional time t^*. It is observed that even with a constant pollutant emission rate, strong fluctuations in time are found. However, a clear difference between beta and gamma radiation is appartent. The concentration (Fig. 2a), and consequently the beta dose rate, is nearly zero except for large peaks which appear at irregular time intervals. The gamma fluence rate on the contrary (Fig. 2b), fluctuates around a mean of 3.5×10^{-6} with maximum deviation of a factor of two from the mean. This is a direct result of integrating the concentration over the whole domain (cf. Eq. 3) as opposed to considering only the local concentration (cf. Eq. 2).

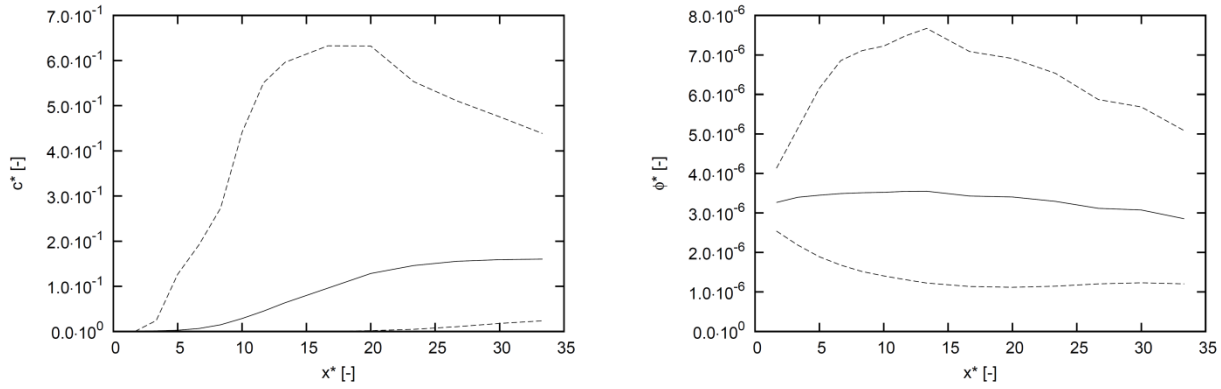

Figure 4: Time-averaged concentration c^* (a) and gamma fluence rate ϕ^* (b) due to ^{133}Xe emission from 75 m altitude ($-$) and 1% - 99% percentiles ($- -$).

The wide spread of the instantaneous concentration signal compared to the gamma fluence rate becomes even more apparent when inspecting the corresponding probability density functions (pdfs). These are provided in Fig. 3a for the concentration, the gamma fluence rate of ^{41}Ar and the gamma fluence rate of ^{133}Xe. For sake of visualization, the gamma fluence rates are rescaled with $U/\lambda L$. The pdf of the concentration stretches from values below 10^6 up to 1 with a maximum probability within 5.0×10^{-4} and 5.0×10^{-2}. This illustrates that the peaks observed in Fig. 2a corresponds to an increase in local dose rate of several orders of magnitude. The pdfs of the gamma fluence rate of ^{41}Ar and ^{133}Xe on the other hand are at lot narrower.

By computing a moving average of the instantaneous fluence rates with an averaging time of $\Delta t = 125$, we obtain the pdfs in Fig. 3b. To illustrate, in case of a release height of 75 m and a wind speed of 22.5 km/h at this altitude, this corresponds to a physical time span of 25 minutes. It is clear that this operation significantly reduces the width of all three pdfs. Nevertheless, the concentration still varies over two orders of magnitude. The gamma fluence rate signal is limited to a very narrow band.

Finally, in Fig. 4, the time-averaged concentration, and gamma fluence rate are shown. In order to illustrate the spread on the instantaneous observations, the 1% and 99% percentiles are also shown in this figure. It is observed that the time-average concentration is essentially zero up to $x^* = 5$. From this point on, the concentration increases up to $x^* = 25$ after which it stabilizes. The time-averaged gamma fluence rate is fairly constant along the stream-wise direction for the range plotted with a value between 2.9×10^{-6} and 3.6×10^{-6}. At larger distance from the source (not shown in this graph), this fluence rate decreases with increasing distance.

The variation on the observations can be quantified by looking at the distance between the 1% - 99% percentiles. A strong dependence of this variation on the distance from the stack is observed for both the concentration and the gamma fluence rate. From the graph it is clear however, that the instantaneous concentration can vary several orders of magnitude with respect to the mean, while 98% of the intantaneous gamma fluence rate observations fall approximately within a factor of two from the mean value. This is particular relevant in situations of short exposure, for example during an evacuation, since these results indicate that the gamma dose measurements from nearby sensors and personal dosimeters cannot be used to accurately estimate the external beta dose. Note that this is also the case for the inhalation dose which also scales with the local concentration (Slade, 1968).

Conclusion

In the current study, we presented a time-dependent dispersion model for the near-range dispersion of radioactive gases in a thermally neutral atmospheric boundary layer. To this end, we coupled a CFD model using LES turbulence modeling with a beta and gamma dose rate model. We argued that the beta dose rate is proportional to the local concentration while the gamma dose rate was computed using the point-kernel method with buildup factors. A set of time-dependent simulations of a constant release of ^{41}Ar and ^{133}Xe into an open field were performed and the dynamics of the external dose rate at ground level due to cloud shine was studied.

A large variation on the beta dose rate is observed, causing peaks in the dose rate of several orders of magnitude. Also the gamma dose rate shows a considerable variability although 98% of the observations fall within a factor of approximately two from the mean value. For both radiation types, time averaging reduces this variability but even for relatively long averaging times the beta dose rate varies over several orders of magnitude. Based on these results we can conclude that a gamma dose assessment at the near-range is not representative for the external beta dose rate and, in extension, neither is it for the inhalation dose rate. However, the model presented in this work provides the means required to estimate an upper boundary to the beta dose received.

References

ANSI 1991 *American National Standard for Gamma-ray Attenuation Coefficients and Buildup Factors for Engineering Materials* ANSI/ANS-6.4.3-1991 (The Society) p 119

Bé M M, et al. (2008) Table of Radionuclides (vol. 4 A=133 to 252). (Sèvres: Bureau International des Poids et Mesures) p 282

Bé M M, et al. (2011) Table of Radionuclides (vol. 6 A=22 to 242). (Sèvres: Bureau International des Poids et Mesures) p 278

Benamrane Y, Wybo J-L and Armand P 2013 Chernobyl and Fukushima nuclear accidents: what has changed in the use of atmospheric dispersion modeling? *Journal of Environmental Radioactivity* **126** 239-52

Berger M J, Coursey J S and Zucker D S 2000 ESTAR, PSTAR, and ASTAR: Computer Programs for Calculating Stopping-Power and Range Tables for Electrons, Protons, and Helium Ions (Version 1.2.2) *National Institute of Standards and Technology*

Bou-Zeid E, Meneveau C and Parlange M B 2005 A scale-dependent Lagrangian dynamic model for large eddy simulation of complex turbulent flows *Physics of fluids* **17**:2 025105

Chamecki M, Meneveau C and Parlange M B 2009 Large eddy simulation of pollen transport in the atmospheric boundary layer *Aerosol Science* **40** 241-55

de Sampaio P, Junior M and Lapa C 2008 A CFD approach to the atmospheric dispersion of radionuclides in the vicinity of NPPs *Nuclear Engineering and Design* **238** 250-73

Nakayama H and Nagai H 2009 Development of Local-Scale High-Resolution Atmospheric Dispersion Model Using Large-Eddy Simulation Part 1: Turbulent Flow and Plume Dispersion over a Flat Terrain *Journal of Nuclear Science and Technology* **46** 1170-7

Punitha G, Sudha A J, Kasinathan N and Rajan M 2008 Atmospheric Dispersion of Sodium Aerosol due to a Sodium Leak in a Fast Breeder Reactor Complex *Journal of Power and Energy Systems* **2** 889-98

Rentai Y 2011 Atmospheric dispersion of radioactive material in radiological risk assessment and emergency response *Progress in Nuclear Science and Technology* **1** 7-13

Slade D H 1968 *Meteorology and atomic energy* (Oak Ridge: US Atomic Energy Commission)

Vach M and Duong V M 2011 Numerical Modeling of Flow Fields and Dispersion of Passive Pollutants in the Vicinity of the Temelín Nuclear Power Plant *Environmental Modeling & Assessment* **16** 135-43

van Kan J 1986 A Second-order Accurate Pressure Correction Scheme for Viscous Incompressible Flow *SIAM Journal on Scientific and Statistical Computing* **7** 870-91

Venkatesan R, Mathiyarasu R and Somayaji K M 2002 A study of atmospheric dispersion of radionuclides at a coastal site using a modied Gaussian model and a mesoscale sea breeze model *Atmospheric Environment* **36**.18 2933-42.

Xie D, Wang H, Kearfott K J, Liu Z and Mo S 2014 Radon dispersion modeling and dose assessment for uranium mine ventilation shaft exhausts under neutral atmospheric stability *Journal of environmental radioactivity* **129** 57-62